Nanoscale

Cite this: *Nanoscale*, 2011, **3**, 4201

www.rsc.org/nanoscale

PAPER

Nanopatterned graphene quantum dots as building blocks for quantum cellular automata

Z. F. Wang and Feng Liu*

Received 13th May 2011, Accepted 24th July 2011
DOI: 10.1039/c1nr10489f

Quantum cellular automata (QCA) is an innovative approach that incorporates quantum entities in classical computation processes. Binary information is encoded in different charge states of the QCA cells and transmitted by the inter-cell Coulomb interaction. Despite the promise of QCA, however, it remains a challenge to identify suitable building blocks for the construction of QCA. Graphene has recently attracted considerable attention owing to its remarkable electronic properties. The planar structure makes it feasible to pattern the whole device architecture in one sheet, compatible with the existing electronics technology. Here, we demonstrate theoretically a new QCA architecture built upon nanopatterned graphene quantum dots (GQDs). Using the tight-binding model, we determine the phenomenological cell parameters and cell–cell response functions of the GQD-QCA to characterize its performance. Furthermore, a GQD-QCA architecture is designed to demonstrate the functionalities of a fundamental majority gate. Our results show great potential in manufacturing high-density ultrafast QCA devices from a single nanopatterned graphene sheet.

Introduction

The miniaturization of the electronic devices is reaching the size limit where the system dynamics is governed by quantum mechanics. As a result, great efforts have been made in looking for different technologies for processing and storing information that can effectively replace the classical electronics.[1–5] QCA[6] is one of the solutions that allows the development of classical computation processes with quantum entities.

Since the initial proposal by the Notre Dame group,[6] QCA has attracted much attention because of its promise of logic circuits with very low power consumption, scalability, and the absence of interconnections.[7–10] QCA is a new computational paradigm, in which the binary information is encoded in the charge state of a cell composed of a small number of QDs. Each QCA cell has two degenerate ground states; the Coulomb interaction between the neighboring cells lifts the degeneracy and results in a "1" or "0" logic state of the cell. The outcome of a logic computation is obtained by enforcing boundary conditions (the controlled input signal) in a two-dimensional array of QCA cells and letting the system relax to its ground state (the binary information is transmitted in this process). Since no current flows between QCA cells, the heat dissipation in the QCA circuit is very low, so it is potentially an ideal approach for building ultra-large scale integrated electronics.

Despite the theoretical merits of QCA, the practical realization of this new computing paradigm has been hindered by the lack of suitable building blocks for QCA cells. Semiconductor technologies that are being considered for the QCA implementation would operate only in cryogenic temperatures due to the large cell size, rendering the conventional QCA[9,10] fail to work at room temperature. The molecular QCA would in principle overcome this difficulty,[11–13] as the small size of molecular QDs makes the Coulomb energies large enough for room temperature operation. However, currently there is no effective process capable of self-organizing molecular QDs at precisely controlled locations. Therefore, the main challenge has been to identify the best candidates of QDs as building blocks for QCA.

Here, we propose a new QCA architecture built upon the nanopatterned GQDs. Using the tight-binding (TB) model, we show that the binary information of QCA can be encoded in different charge states of the coupled GQDs. We derive the phenomenological cell parameters of the GQD-QCA and characterize its operation performance from the calculated cell–cell response function. Furthermore, a QCA array that serves as the fundamental (NOR and NAND) majority gate is designed for evaluation. Since GQD-QCA can be potentially made by nanopatterning techniques compatible with the existing electronics technology,[14–17] our results show great promise for constructing high-density ultrafast GQD-QCA devices.

Results and discussion

The basic requirement for constructing the QCA device is to design a QCA cell that contains bistable charge states for storing the "0" and "1" binary information. One way to create the GQDs is to construct a semiconductor–metal–semiconductor (SMS)

Department of Materials Science and Engineering, University of Utah, Salt Lake City, UT 84112, USA. E-mail: fliu@eng.utah.edu

graphene nanoribbon (GNR) junction,[18] as shown in Fig. 1a, where the width and length of the GQD are labeled by integer W and M_1. The electronic structure of such GQD is calculated by the nearest-neighbor (NN) π-orbital TB model with hopping parameter $\gamma = 2.66$ eV. The density of state (DOS) is determined by direct diagonalization of the Hamiltonian $H = H_c + \sum_L^r + \sum_R^r$, where H_c is the Hamiltonian of the GQD (zigzag GNR), $\sum_L^r$ and $\sum_R^r$ are self-energy contributions from the left and right leads (armchair GNRs). We note that Guo *et al.*[19] have shown that including higher-order hopping parameters in the TB model will break the electron-hole symmetry, but will not remove the QD states inside the gap, which is consistent with previous DFT results.[20] Fig. 1b shows the density of state (DOS) of the GQD with $W = 7$ and $M_1 = 3$. There are two confined states (QD states) within the energy band gap, indicating that such SMS junction can be used as a QD. The number of QD states increases with the increasing width/length of the SMS GNR junction,[18] but we can always have one electron to occupy the lowest unoccupied QD state by adjusting the Fermi level through the back gate.

It is straightforward to extend the design of single GQD to two coupled GQDs, as shown in Fig. 1c. If one extra electron is added to the system, it can occupy either one of the QDs, leading to two degenerate ground states that constitute the bistable charge states of a QCA cell. The DOS of the QCA cell (two coupled GQDs, $W = 7$, $M_1 = 3$ and $M_2 = 3$) is shown in Fig. 1d. Comparing to Fig. 1b, the single QD state is split into two hybrid QD states due to the coupling between the two QDs. The wavefunctions (ψ_1 and ψ_2) of the hybrid QD states with energy E_1 and E_2 are shown in Fig. 2a and b. Recombining these two hybrid states, we obtain the non-interacting QD states ($\psi_{dot1} = (\psi_1 - \psi_2)/\sqrt{2}$ and $\psi_{dot2} = (\psi_1 + \psi_2)/\sqrt{2}$), which are localized at the right and left junction region, respectively, as shown in Fig. 2c and d.

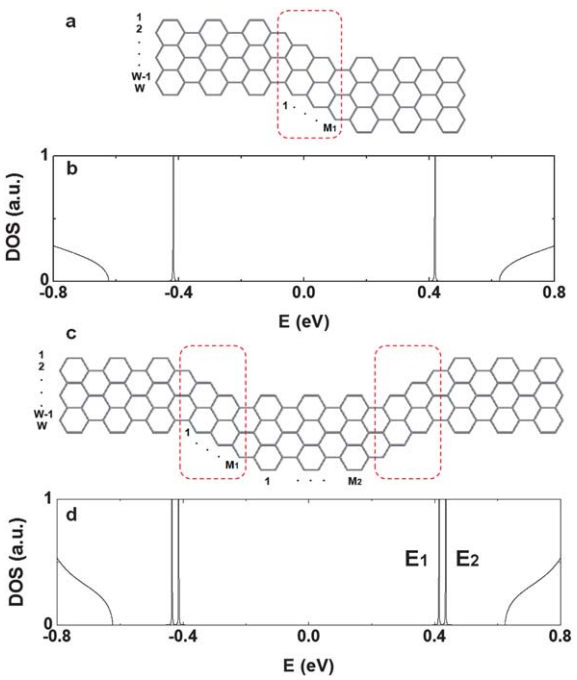

Fig. 1 Single and coupled GQDs. (a and c) Schematic of the single and coupled GQDs, W and M_1 denote the width and length of the QD, M_2 denotes the apparent inter-dot distance, and the dashed rectangles enclose the QD region. (b and d) Density of state of the single and coupled GQDs with $W = 7$, $M_1 = 3$ and $M_2 = 3$. E_1 and E_2 denote the energy of the hybrid QD states.

The QCA cell state can be represented by three cell parameters: the charging energy (on-site energy), the inter-dot coupling energy (hopping energy) and the effective inter-dot distance, which are defined as[21] $E_0 = (E_2 + E_1)/2$, $t = (E_2 - E_1)/2$ and $R = 1/[\sum_{\vec{r}_1,\vec{r}_2} |\psi_{dot1}(\vec{r}_1)|^2 |\psi_{dot2}(\vec{r}_2)|^2 / |\vec{r}_1 - \vec{r}_2|]$, respectively. The dependence of these cell parameters on the apparent inter-dot distance (M_2) is shown in Fig. 3. The charging energy and the inter-dot coupling energy decrease monotonically with the increasing M_2, while the effective inter-dot distance increases linearly with the increasing M_2. The inter-dot coupling energy is determined by the wavefunction overlap between the two non-interacting QD states, which are mainly localized at the zigzag junction region (see Fig. 2c and d). As the overlap decreases with the increasing M_2, so does the inter-dot coupling energy. Meantime, the QD charging energy gradually decreases towards the value of single isolated QD as the inter-dot coupling energy decreases.

Using these cell parameters, we can further illustrate the relationship between the geometric structures of the GQDs and QCA cells, and construct a simple phenomenological model to describe the functionality of QCA arrays,[21] *i.e.* calculating the ground state charge distribution in QCA arrays under the enforcing boundary conditions. In our work, we use the two-dot QCA cells, rather than the more common four-dot cells studied in previous theoretical works. In the Hilbert space spanned by the two non-interacting QD states (ψ_{dot1} and ψ_{dot2}), the Hamiltonian of the QCA cell (two coupled GQDs) can be written as

$$H_0^{cell} = \sum_{i=1,2} E_0 n_i + t\left(a_1^+ a_2 + a_2^+ a_1\right). \quad (1)$$

Here a_i^+, a_i and $n_i = a_i^+ a_i$ are the creation, annihilation and number operators for an electron at QD i ($i = 1, 2$). If many QCA cells are put together, the potential distribution at one dot in a given cell will depend on the charge density at every dot in all

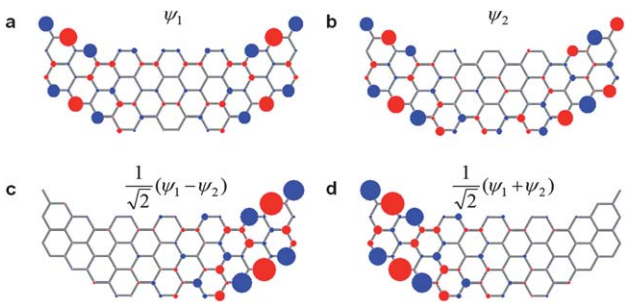

Fig. 2 Wavefunctions of the hybrid and non-interacting QD states in a two-dot QCA cell. (a and b) Wavefunctions of the hybrid QD states with energy E_1 and E_2 shown in Fig. 1d. (c and d) Wavefunctions of the non-interacting QD states constructed from the linear combination of the two hybrid QD states. The radii of the circles around each atom correspond to the absolute values of the wavefunction, red (blue) indicates positive (negative) sign.

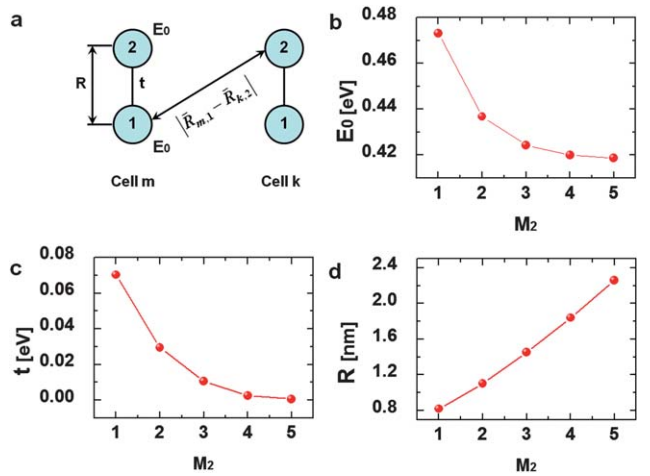

Fig. 3 Phenomenological GQD-QCA cell parameters. (a) Schematic of QCA cells and cell parameters. (b) Charging energy, (c) inter-dot coupling energy and (d) effective inter-dot distance as a function of the apparent inter-dot distance M_2 (see Fig. 1c). The width and length of the QD are $W = 7$ and $M_1 = 3$.

other cells. Beginning with an initial guess for the densities in all the cells, the perturbation Hamiltonian potential of the cell k due to the charges in all other cells is given by

$$H_k^{\text{cell}} = \sum_{i=1,2} V_i^k n_i = \sum_{i=1,2}\left[\sum_{m\neq k,j} \frac{e^2}{4\pi\varepsilon}\frac{\rho_j^m - \bar{\rho}}{|\vec{R}_{m,j} - \vec{R}_{k,i}|}\right] n_i. \quad (2)$$

Here V_i^k is the potential at dot i in the cell k. We denote the position of dot j in the cell m as $\vec{R}_{m,j}$ (Fig. 3a), and the single-particle density at QD j in the cell m as ρ_j^m. To maintain charge neutrality, a fixed positive charge $\bar{\rho} = 0.5$ is assumed at each dot. Solving the Schrödinger equation for each cell,

$$E|\psi_0^k\rangle = (H_0^{\text{cell}} + H_k^{\text{cell}})|\psi_0^k\rangle, \quad (3)$$

we obtain the ground-state wavefunction at zero degree of temperature. From the ground-state wavefunctions, the new single-particle densities are calculated as

$$\rho_{1,2}^k = \langle\psi_0^k|n_{1,2}|\psi_0^k\rangle. \quad (4)$$

Eqn (1)–(4) are self-consistently solved until the converged ground-state charge density is obtained. To describe the charge distribution in each QCA cell, we adopt the quantity of cell polarization[1] to measure the relative charge occupation in the two QDs within a cell. The polarization of the cell k is defined as $P_k = (\rho_1^k - \rho_2^k)/(\rho_1^k + \rho_2^k)$, where ρ_1^k (ρ_2^k) is the charge density at QD 1 (2) in the cell k. If one electron is entirely localized on QD 1, then $P_k = 1$; if the electron is on QD 2, then $P_k = -1$. Without Coulomb interaction with other cells, an isolated cell would have a ground state consisting of a linear combination of these two polarizations with a net polarization of zero.

Once the binary information is available to us, we must be able to transmit it as well. We may define the $P > 0$ and $P < 0$ state as the bit value of "1" and "0", respectively, to transmit the binary information between the two cells. The charge state in one cell can be switched by a neighboring cell through the inter-cell Coulomb interaction. Consider two QCA cells adjacent to each other. Suppose we fix the polarization of the driver cell to P_1, what is the polarization of the responder cell P_2? To answer this question, we have calculated the cell–cell response functions for different QCA cell architectures. In case one, two QCA cells are aligned vertically next to each other, as shown in Fig. 4a. We calculate P_2 as a function of P_1 for the fixed apparent inter-dot distance ($M_2 = 5$, see Fig. 1c) and a changing inter-cell distance (L_1, see Fig. 4a). The polarizations of the two cells (P_1 and P_2) are opposite to each other, as the electron prefers to occupy the different QDs in the neighboring cells due to the Coulomb repulsion. In addition, the response function is highly non-linear, a very small polarization of the driver cell P_1 will induce nearly complete polarization of the responder cell P_2 (Fig. 4b). Such abrupt polarization response function is highly desirable for storing the bit information, because it ensures the bit value to be encoded unambiguously. We may also fix the inter-cell distance ($L_1 = 1$ nm) and change the apparent inter-dot distance (M_2). As shown in Fig. 4c, for small M_2, P_2 shows a linear relation with P_1, *i.e.* a larger polarization of the driver cell is needed to induce a high polarization of the responder cell. With the increasing M_2, this response function becomes more and more non-linear, *i.e.* a small polarization of the driver cell is sufficient to induce a high polarization of the responder cell. In case two, two QCA cells are aligned horizontally next to each other, as shown in Fig. 4d. Now the polarizations of the two cells (P_1 and P_2) have the same direction, *i.e.* the electron prefers to occupy the same (left or right) dot in each cell. On the other hand, the response functions (Fig. 4e and f) behave qualitatively the same as those in the vertical arrangement of QCA cells (Fig. 4b and c). From Fig. 4, we see that there are two important factors in determining the performance of QCA. First, the inter-dot coupling energy (governed by the inter-dot distance) should be small enough to yield strong bistable behavior of each QCA cell. Second, the inter-cell Coulomb interaction (governed by the inter-cell distance) should be large enough to yield the complete polarization of the responder cells.

After establishing the response function between two QCA cells, we can further calculate the response function of a QCA array consisting of many cells, as shown in Fig. 5. Again the QCA cells may be aligned either vertically (Fig. 5a) or horizontally (Fig. 5c). We are interested in the question that given the polarization of the driver cell, if the inter-cell Coulomb interaction is strong enough to polarize the whole array, so that the binary information can be transmitted from one place to another. Fig. 5b shows the polarization as a function of cell number for the vertical QCA array containing five cells (Fig. 5a). The polarization of the driver cell is set to values $P_1 = 1.0, 0.8, 0.6$ and 0.4, respectively. The ground state of the electrons in the remaining four cells is calculated. Note that the polarization oscillates between 1 and -1 from the second to the fifth cell, which are completely polarized for all the input polarizations of the driver cell. It indicates that the binary information is transmitted without damping in the vertical QCA array (Fig. 5a). Similar behavior is also observed in the horizontal QCA array (Fig. 5c). The polarization reaches quickly to 1 from the second cell on, as shown in Fig. 5d. However, if the inter-dot distance is decreased or the inter-cell distance is increased, the performance of the QCA array is seen to decay (not shown). Therefore, by designing the QCA array and the architecture with appropriate

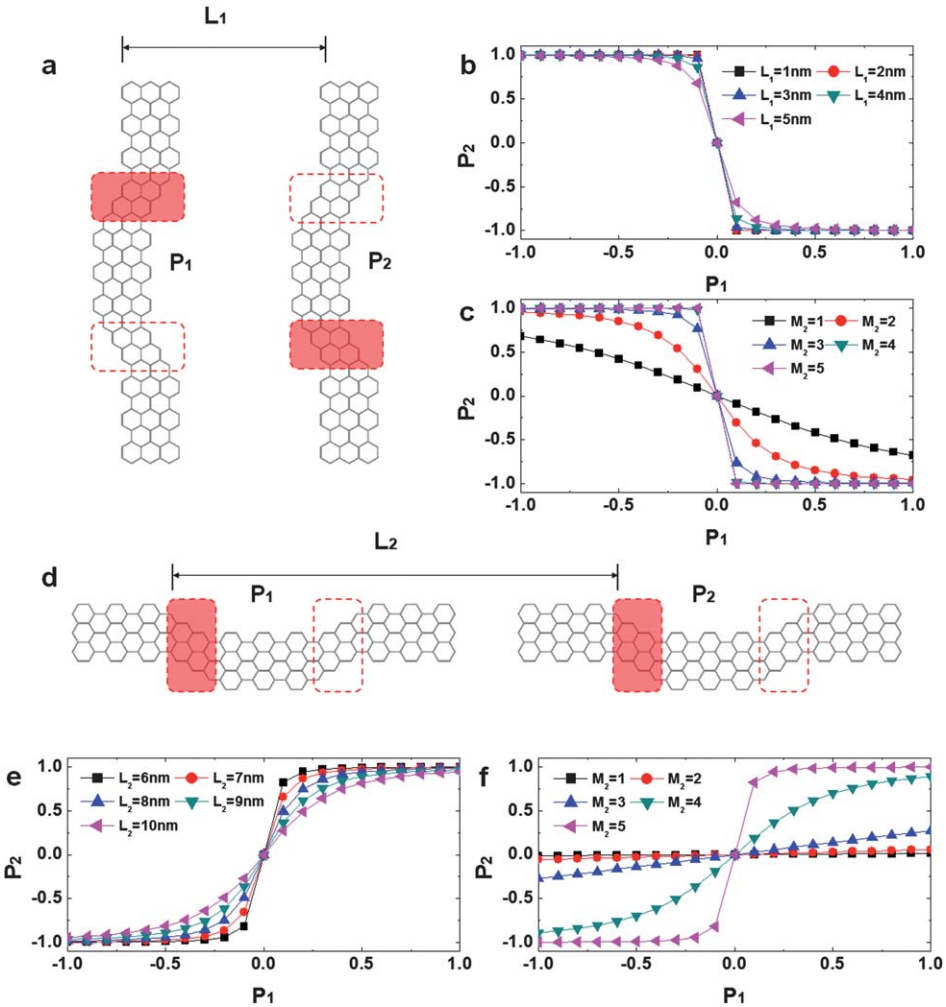

Fig. 4 Response function of two QCA cells. (a and d) Schematic of two QCA cells in the vertical and horizontal arrangement. L_1 and L_2 are the inter-cell distance, P_1 and P_2 are the polarization of the driver and responder cell, respectively. Filled (empty) rectangles denote the occupation (unoccupation) of the electron. (b and c) Response functions of QCA in (a) with $W = 7$, $M_1 = 3$, $M_2 = 5$ and $W = 7$, $M_1 = 3$, $L_1 = 1$ nm, respectively. (e and f) Response functions of QCA in (d) with $W = 7$, $M_1 = 3$, $M_2 = 5$ and $W = 7$, $M_1 = 3$, $L_2 = 6$ nm, respectively.

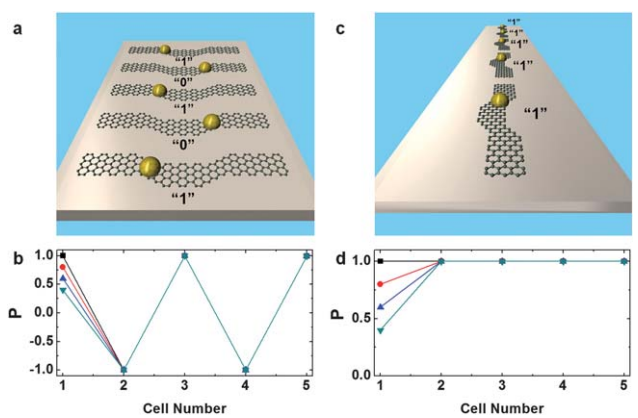

Fig. 5 Response function of a QCA array. (a and c) Schematic of five QCA cells in the vertical and horizontal arrangement. The ball in the GQD region denotes the occupation of electron, "1" and "0" label the bit information. (b) Response function of the vertical-cell QCA with $W = 7$, $M_1 = 3$, $M_2 = 5$, $L_1 = 5$ nm. (d) Response function of the horizontal-cell QCA with $W = 7$, $M_1 = 3$, $M_2 = 5$, $L_2 = 8$ nm.

inter-dot and inter-cell distances, high performance of binary information transmission can be achieved.

To further demonstrate the validity of GQD-QCA, we finally show a simple design of the GQD-QCA majority gate (NOR and NAND). As shown in Fig. 6, four QCA cells are arranged in T-shape architecture. The polarization of the central cell is assigned as the output (Out), the polarization of the left and right cell is assigned as operands B and C, respectively, and that of the top cell as a programming bit A. We input the polarization of cells A, B and C, and calculate the resulting electron ground state (polarization) of the central cell. The truth table of the programmable majority gate, *i.e.* the input and output polarizations, is shown in Table 1. If A is programmed as "1", the logic is $Out = \overline{B \cap C}$, a NAND gate; if A is programmed as "0", the logic is $Out = \overline{B \cup C}$, a NOR gate. These are two fundamental gates, from which all other gates can be constructed. This scheme therefore provides, in principle, an effective design for all digital logic operations.

Unlike nanotube, GQD devices will most likely have irregularities and defects on the edges.[22] In our previous work,[18] we

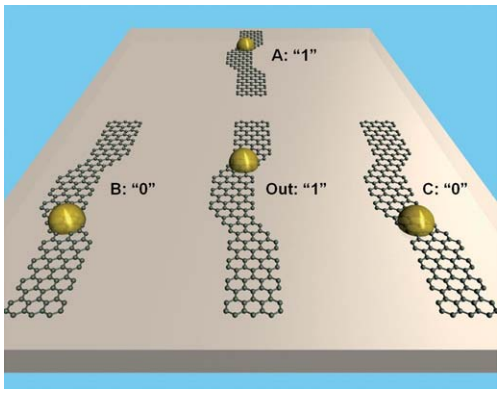

Fig. 6 A QCA majority gate. Schematic of four QCA cells in the T-shape arrangement as a majority gate. $W = 7$, $M_1 = 3$, $M_2 = 5$, $L_1 = 5$ nm, $L_2 = 8$ nm. A, B and C are the input bits, Out is the output bit. Polarization labels are the same as those in Fig. 5.

Table 1 Truth table of the programmable majority gate. The input and output polarizations are listed in the brackets

Logic gate	A (P)	B (P)	C (P)	Out (P)
NAND $Out = \overline{B \cap C}$	"1" (1)	"1" (1)	"1" (1)	"0" (−0.997)
		"0" (−1)	"0" (−1)	"1" (0.999)
		"1" (1)	"0" (−1)	"1" (0.985)
		"0" (−1)	"1" (1)	"1" (0.985)
NOR $Out = \overline{B \cup C}$	"0" (−1)	"1" (1)	"1" (1)	"0" (−0.999)
		"0" (−1)	"0" (−1)	"1" (0.997)
		"1" (1)	"0" (−1)	"0" (−0.985)
		"0" (−1)	"1" (1)	"0" (−0.985)

have demonstrated that the QD states still exist even under the presence of the irregular edges. However, the energy positions of these QDs are sensitive to the edge profile. When two QDs are coupled together, the corresponding QCA cell parameters will also depend on the edge profile, and it is equivalent to an imperfect QCA cell. Several researchers have investigated fault tolerance properties and robustness of QCA logic gates by considering imperfect QCA cells.[23–25] So, it would be interesting to carry out similar studies for the proposed GQD QCA cells in the future.

Conclusion

Our studies show that it is possible to transmit binary information and realize the logic operation through GQD-QCA. The basic element of QCA is a cell with two coupled GQDs. It is worth to point out that GQD construction should not be limited to the SMS GNR junctions as we presented here, other graphene nanostructures may also be utilized as QD building blocks for QCA. For example, if two graphene nanoflakes are connected together, it forms a two-QD QCA cell. In fact, the graphene nanoflake has already been studied as QD for the Coulomb blockage effect in the experiment.[26,27] The flexibility in designing graphene based QCA cell provides more freedom for experimental fabrication. In addition, for reading and writing binary information, the QCA devices must be connected with external circuits. This can be difficult for the molecular QCA device, because there exists usually a large contact resistance between the metal electrodes and molecules due to the very small contact area. However, the GQD-QCA devices may circumvent this difficulty, because they can be easily connected to the outside circuits exclusively *via* metallic GNRs, which serve as extensions of metal electrodes to make contact with the QCA, so as to minimize the contact resistance.[15] These additional advantages merit the nanopatterned GQDs even more attractive as building blocks for QCA.

Acknowledgements

This work was supported by DOE-BES and CMSN programs. We thank Center for High Performance Computing at the University of Utah for providing the computing resources.

References

1 R. H. Hadfield, *Nat. Photonics*, 2009, **3**, 696–705.
2 A. I. Lvovsky, B. C. Sanders and W. Tittel, *Nat. Photonics*, 2009, **3**, 706–714.
3 B. Trauzettel, D. V. Bulaev, D. Loss and G. Burkard, *Nat. Phys.*, 2007, **3**, 192–196.
4 I. Žutić, J. Fabian and S. D. Sarma, *Rev. Mod. Phys.*, 2004, **76**, 323–410.
5 S. A. Wolf, D. D. Awschalom, R. A. Buhrman, J. M. Daughton, S. V. Molnár, M. L. Roukes, A. Y. Chtchelkanova and D. M. Treger, *Science*, 2001, **294**, 1488–1495.
6 C. S. Lent, P. D. Tougaw, W. Porod and G. H. Bernstein, *Nanotechnology*, 1993, **4**, 49–57.
7 A. Imre, G. Csaba, L. Ji, A. Orlov, G. H. Bernstein and W. Porod, *Science*, 2006, **311**, 205–208.
8 R. P. Cowburn and M. E. Welland, *Science*, 2000, **287**, 1466–1468.
9 I. Amlani, A. O. Orlov, G. Toth, G. H. Bernstein, C. S. Lent and G. L. Snider, *Science*, 1999, **284**, 289–291.
10 A. O. Orlov, I. Amlani, G. H. Bernstein, C. S. Lent and G. L. Snider, *Science*, 1997, **277**, 928–930.
11 Y. Lu, M. Liu and C. S. Lent, *J. Appl. Phys.*, 2007, **102**, 034311.
12 C. S. Lent, B. Isaksen and M. Lieberman, *J. Am. Chem. Soc.*, 2003, **125**, 1056–1063.
13 J. Jiao, G. J. Long, F. Grandjean, A. M. Beatty and T. P. Fehlner, *J. Am. Chem. Soc.*, 2003, **125**, 7522–7523.
14 C. Berger, Z. Song, X. Li, X. Wu, N. Brown, C. Naud, D. Mayou, T. Li, J. Hass, A. N. Marchenkov, E. H. Conrad, P. N. First and W. A. D. Heer, *Science*, 2006, **312**, 1191–1196.
15 Q. Yan, B. Huang, J. Yu, F. Zheng, J. Zang, J. Wu, B. Gu, F. Liu and W. Duan, *Nano Lett.*, 2007, **7**, 1469–1473.
16 W. Liu, Z. F. Wang, Q. W. Shi, J. Yang and F. Liu, *Phys. Rev. B: Condens. Matter Mater. Phys.*, 2009, **80**, 233405.
17 Z. F. Wang and F. Liu, *ACS Nano*, 2010, **4**, 2459–2465.
18 Z. F. Wang, Q. W. Shi, Q. Li, X. Wang, J. G. Hou, H. Zheng, Y. Yao and J. Chen, *Appl. Phys. Lett.*, 2007, **91**, 053109.
19 G. P. Guo, Z. R. Lin, T. Tu, G. Cao, X. P. Li and G. C. Guo, *New J. Phys.*, 2009, **11**, 123005.
20 H. Ren, Q. Li, Q. W. Shi and J. Yang, *Chin. J. Chem. Phys.*, 2007, **20**, 489–494.
21 H. Wu and D. W. L. Sprung, *J. Appl. Phys.*, 1998, **84**, 4000–4005.
22 B. Huang, F. Liu, J. Wu, B. Gu and W. Duan, *Phys. Rev. B: Condens. Matter Mater. Phys.*, 2008, **77**, 153411.
23 M. Khatun, T. Barclay, I. Sturzu and P. D. Tougaw, *J. Appl. Phys.*, 2005, **98**, 094904.
24 M. Khatun, T. Barclay, I. Sturzu and P. D. Tougaw, *J. Phys. D: Appl. Phys.*, 2006, **39**, 1489–1494.
25 G. A. Anduwan, B. D. Padgett, M. Kuntzman, M. K. Hendrichsen, I. Sturzu, M. Khatun and P. D. Tougaw, *J. Appl. Phys.*, 2010, **107**, 114306.
26 L. A. Ponomarenko, F. Schedin, M. I. Katsnelson, R. Yang, E. W. Hill, K. S. Novoselov and A. K. Geim, *Science*, 2008, **18**, 356–358.
27 J. Güttinger, C. Stampfer, S. Hellmüller, F. Molitor, T. Ihn and K. Ensslin, *Appl. Phys. Lett.*, 2008, **93**, 212102.